An Underlay Communication Channel for 5G Cognitive Mesh Networks: Packet Design, Implementation, Analysis, and Experimental Results

IEEE International Conference on Communications (IEEE ICC 2016)

Tarek Haddadin, Stephen Andrew Laraway,
Arslan Majid, Taylor Sibbett,
Behrouz Farhang-Boroujeny

(University of Utah)

Daryl Leon Wasden

(Colmek, Inc.)

Brandon F. Lo, Lloyd Landon, David Couch,
Hussein Moradi

(Idaho National Laboratory)

April 2016

Idaho National Laboratory

An Underlay Communication Channel for 5G Cognitive Mesh Networks: Packet Design, Implementation, Analysis, and Experimental Results

Tarek Haddadin[†], Stephen Andrew Laraway[†], Arslan Majid[†], Taylor Sibbett[†], Daryl Leon Wasden[+],
Brandon F. Lo[‡], Lloyd Landon[‡], David Couch[‡], Hussein Moradi[‡], and Behrouz Farhang-Boroujeny[†]
[†]ECE Department, University of Utah, Salt Lake City, UT 84112
[+]Colmek Inc., Salt Lake City, UT 84104
[‡]Idaho National Laboratory, Idaho Falls, ID 83415

Abstract—**This paper proposes and presents the design and implementation of an underlay communication channel (UCC) for 5G cognitive mesh networks. The UCC builds its waveform based on filter bank multicarrier spread spectrum (FB-MC-SS) signaling. The use of this novel spread spectrum signaling allows the device-to-device (D2D) user equipments (UEs) to communicate at a level well below noise temperature and hence, minimize taxation on macro-cell/small-cell base stations and their UEs in 5G wireless systems. Moreover, the use of filter banks allows us to avoid those portions of the spectrum that are in use by macro-cell and small-cell users. Hence, both D2D-to-cellular and cellular-to-D2D interference will be very close to none. We propose a specific packet for UCC and develop algorithms for packet detection, timing acquisition and tracking, as well as channel estimation and equalization. We also present the detail of an implementation of the proposed transceiver on a software radio platform and compare our experimental results with those from a theoretical analysis of our packet detection algorithm.**

I. INTRODUCTION

Cognitive radios optimize the usage of a given spectrum by utilizing a spectrum sharing paradigm known as dynamic spectrum access (DSA). Traditionally, primary users were granted exclusive access to a broadband of spectrum in order to guarantee negligible interference from other users. This standard leads to poor utilization of the spectrum by allowing a spectral band to remain vacant when its assigned user is idle. DSA, on the other hand, allows secondary users to share the spectrum with the primary users and utilize vacant bandwidth when available. In order to access and exit the spectrum dynamically based on the primary users' activity, the secondary users must actively sense their surrounding environment and subsequently share their findings with neighboring users. Alternatively, in cases when the spectrum usage is reasonably static (e.g., TV White spaces), a geolocation database may be a preferred choice [1], [2]. It should be noted, however, that additional cooperation among the secondary user nodes in this scenario also results in a more efficient usage of the spectrum [3].

Spectrum sensing has received broad attention in the past and well-established approaches have been reported in the literature, e.g., [4]–[8]. Standard methods to make use of geolocation databases have also been well studied. The more challenging task is to find an effective method for exchanging the sensed information among the nodes within the secondary network and, accordingly, assigning spectra for communications. Such an exchange of information clearly requires a communication channel, commonly referred to as a control channel [9], for cooperation among cognitive radio users.

In 5G wireless systems, device-to-device (D2D) communications [10] enable user equipments (UEs) of multi-tier cells to communicate and cooperate with each other directly in a mesh network. The realization of D2D communications in 5G cognitive mesh networks must overcome three primary issues: i) readily available control resources for cooperation, ii) D2D-to-cellular interference (and its converse), and iii) D2D-to-D2D interference. In order to facilitate user cooperation, numerous mesh network operations require an "always on" control channel for reliable control transmissions. These network operations include beaconing, neighbor discovery, synchronization, channel access negotiations, route setup and updates, and cooperative spectrum sensing [9]. The minimization of D2D-to-cellular interference and cellular-to-D2D interference is crucial in order to achieve reliable communication in both instances. Additionally, the lack of cooperation among the D2D UEs leads to the challenge of D2D-to-D2D interference. It is noted that cooperation can be achieved, but at high cost by using precious macro-cell/small-cell control resources. To resolve these issues, an appealing choice is an underlay channel, which allows continuous access by D2D UEs for cooperation and interference management provided that the interference to other cellular users remains below the noise temperature. Spread spectrum techniques are an obvious choice for such an underlay system as their transmit power spectral density (PSD) is maintained at a level comparable to or below the noise floor. In this paper, we refer to this communication strategy as underlay communication channel (UCC).

Although direct sequence spread spectrum (DS-SS) and frequency hopping spread spectrum (FH-SS) are the most widely established spread spectrum techniques, filter bank multicarrier spread spectrum (FB-MC-SS) is a more appealing approach for the UCC. FB-MC-SS is significantly more robust

to narrow-band and partial-band interference [11]–[15], and the presence of primary users may be viewed as partial-band interference [16]. In FB-MC-SS, a transmit data stream is spread over a number of subcarriers and its PSD is maintained at a level below the noise temperature. Upon detection of the activity of macro-cell users and other UEs, the subcarriers that coincide with these transmissions may be turned off in order to increase the reliability of the UCC and simultaneously decrease its impact on these users.

The presentation in [16] was centered around a few fundamental features of FB-MC-SS, without paying detailed attention to a practical implementation of the proposed UCC. In this paper, we report our recent progress in completing the design and fine tuning of FB-MC-SS to allow for the implementation of the UCC. Our proposed UCC is "always on" and robust to interference due to its filter bank structure and underlay approach. More importantly, it provides the physical layer packet detection and timing acquisition mechanisms to achieve reliable reception, accurate detection, and correct decoding of these control messages with high probability of detection and low probability of false alarm. Our contributions are as follows:

- We propose an underlay communication channel based on FB-MC-SS to facilitate D2D communications and cooperation among D2D UEs in 5G cognitive mesh networks.
- We present a new packet format that is tailored towards a simple and effective implementation in order to allow reliable communication in a mesh network.
- We propose a novel timing acquisition and packet detection method which utilizes a *maximum-based* passive-search scheme.
- We confirm the accuracy of the theoretical false alarm and missed detection probabilities, presented in [17], using our experimental system.
- We discuss issues related to carrier synchronization and tracking of channel variation during each packet, and present solutions to these issues.
- We implement and evaluate our design on a software defined radio.
- We show our design occupies only 50% of a Xilinx Kintex 7 FPGA chip, hence, confirm its practicality for D2D applications.

The rest of this paper is organized as follows. Section II presents a brief summary of the FB-MC-SS waveform and its main features. Section III presents the proposed FB-MC-SS packet and its prominent features related to our implementation. Section IV contains a mathematical analysis of our chosen preamble. Section V describes the proposed packet detection and timing acquisition algorithm. Section VI presents implementation details of the FB-MC-SS transmitter and receiver. Section VII presents experimental results that confirm our theoretical analysis. Section VIII discusses the applications of our UCC design in 5G cognitive mesh networks. Section IX presents the concluding remarks of the paper.

preamble	payload indicator	payload
$+1, -1, \cdots, +1, -1$	XXXXX	DDDDDDDDD $\cdots$ DDDDDDDDD
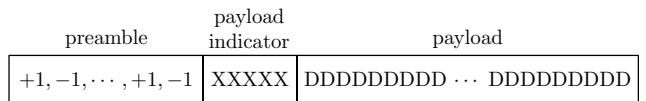
Fig. 1. Proposed packet format.

II. FB-MC-SS Waveform

In FB-MC-SS of [16], the transmit signal is constructed according to the equation

$$x(t) = s(t) \star g(t) \tag{1}$$

where $\star$ denotes linear convolution, $s(t) = \sum_n s[n]\delta(t - nT)$ is a train of impulses carrying the data symbols $s[n]$, T is the symbol interval, $g(t) = \sum_{k=0}^{N-1} h_k(t)$ is the transmit pulse-shape, N is the number of subcarriers, $h_k(t) = \gamma_k h(t)e^{j2\pi f_k t}$ is the pulse-shape associated with the kth subcarrier, γ_k are a set of spreading gains (in the form of $\gamma_k = e^{j\theta_k}$), f_k are the subcarrier frequencies, and $h(t)$ is a square-root Nyquist pulse-shape. In [16], $h(t)$ is chosen to be a square-root raised-cosine pulse with a roll-off factor $\alpha = 1$. One may notice that the specified roll-off factor leads to 100% excess bandwidth in a typical single user system, leading to an inefficient usage of bandwidth. The theoretical analysis presented in [16] shows that this choice of α has an insignificant impact on bandwidth efficiency of FB-MC-SS. In return, it allows the choice of a prototype filter with minimal out-of-band spectral leakage. Lastly, the subband center frequencies are positioned at $f_k = \pm 1/T, \pm 3/T, \cdots, \pm(N-1)/T$.

III. Packet Format

Each packet in UCC begins with a preamble and an indicator/control word, followed by the information payload. The preamble is used for timing acquisition, carrier frequency offset estimation, channel estimation, and noise variance estimation. These will be used to set up the receiver for an optimum detection of the data symbols in the payload. The indicator/control word is used to confirm the validity of the packet detection, and determine where the payload begins.

For the preamble, we use a train of symbols that toggle between $+1$ and -1. The preamble is assumed to be of length W_{pa} symbols, where W_{pa} is an even integer, and the payload is of fixed length W_{pl} symbols. Fig. 1 depicts the proposed packet format.

IV. Mathematical Analysis of Preamble

During the preamble period of the packet format proposed in Section III, we have

$$s(t) = \sum_n (-1)^n \delta(t - nT). \tag{2}$$

We observe that this choice of $s(t)$ is a periodic function with a period of $2T$. It thus can be expanded by its Fourier series, leading to

$$s(t) = \frac{1}{T} \sum_{k=-\infty}^{\infty} e^{j\frac{(2k+1)\pi}{T}t}. \tag{3}$$

This indicates that $s(t)$ is a summation of infinite tones at frequencies $\{f = \frac{(2k+1)}{2T}, -\infty < k < \infty\}$. When $s(t)$ is passed through the transmit pulse-shaping filter and subsequently through the channel, those tones that are within the band of transmission will be retained and the rest will be removed. The receiver first demodulates the received signal to baseband, yielding $y(t)$, and passes it through a matched filter $g^*(-t)$. After straight-forward derivations, one finds the signal at the matched filter output to be

$$y'(t) = \frac{1}{2}\left(\sum_{k=-N}^{N-1} e^{j\frac{(2k+1)\pi}{T}t}\right) \star c(t) + v'(t) \qquad (4)$$

where $c(t)$ is the channel impulse response and $v'(t)$ is the filtered channel noise.

Noting that the summation enclosed by parentheses in (4) is a truncated (equivalently, rectangular windowed) version of the summation in (3), we rewrite (4) as

$$y'(t) = \left(\sum_n (-1)^n N \mathrm{sinc}\left(\frac{t-nT}{T/(2N)}\right)\right) \star c(t) + v'(t). \quad (5)$$

To have a better understanding of this result, consider the case where $c(t) = \delta(t)$, i.e., there is only a line of sight path with the gain of unity. In that case, (5) reduces to

$$y'(t) = \sum_n (-1)^n N \mathrm{sinc}\left(\frac{t-nT}{T/(2N)}\right) + v'(t). \qquad (6)$$

We note that the sinc pulses have the main lobe width of T/N. For typical choices of N, this is a relatively narrow pulse. Accordingly, one may think of the sinc pulses as an approximation to a sequence of impulses and, hence, (5) resembles the preamble sequence (2). The gain factor N in front of the sinc pulses arises from the processing gain of the matched filter.

V. Packet Detection and Timing Acquisition Algorithm

To introduce our packet detection and timing acquisition methods, and present an analysis of their expected performance, we limit our presentation to the case where $c(t) = \delta(t)$. The developed results are trivially extendable to the case where the channel consists of a number of multipaths clustered in a time span that is a small fraction of one symbol period, T. Also, since the receiver is implemented based on samples of the received signal, we continue our discussion starting with the following sampled version of (6):

$$y'[n] = \sum_k (-1)^k N \mathrm{sinc}\left(\frac{n-kL}{L/(2N)}\right) + v'[n]. \qquad (7)$$

Here, L denotes the number of samples within a symbol period of T seconds. According to (7), the transmit sequence of alternating $+1$ and -1 preamble symbols buried in background noise have been recovered and amplified with a gain of N by the matched filter for packet detection and timing acquisition.

The purpose of the packet detection is to process the signal samples in (7) and identify a consistent presence of

---

Algorithm 1 Packet Detection
> **INPUT:** $y'[n]$
> **OUTPUT:** $packet\_det$
> **INITIALIZE:** $w = 0, \mathbf{Z} = \mathbf{0}, \boldsymbol{\tau} = \mathbf{0}, packet\_det = 0$
> 1: **while** $packet\_det \neq 1$ **do**
> 2:   **for** $n = wL, wL+1, \cdots, wL+L-1$ **do**
> 3: $z[n] = |y'[n]|^2$
> 4: $\mathbf{Z}(n, w) = z[n]$
> 5:   **end for**
> 6: $[z_w^{\max}, \tau_w^{\max}] = \max(\mathbf{Z}(:, w))$
> 7: $\boldsymbol{\tau}(0 : M-1) = [\boldsymbol{\tau}(1 : M-1) \quad \tau_w^{\max}]$
> 8:   **if** K out of M elements in $\boldsymbol{\tau}$ are equal **then**
> 9: $packet\_det = 1$
> 10:   **end if**
> 11: $w = (w + 1) \mod M$
> 12: **end while**

---

alternating $+N$ and $-N$ samples. The timing acquisition, then, takes the position of these samples as the correct timing phase for the rest of the processing steps at the receiver. An effective algorithm that accomplishes these tasks is shown in Algorithm 1.

In Algorithm 1, we first find $z[n]$, the magnitude square of the matched filter output y'[n] (line 3). We then insert $z[n]$ into row n and column w of matrix $\mathbf{Z}$ (line 4), and find the maximum value, $z_w^{\max}$, and the row index of this maximum value, $\tau_w^{\max}$, in column w of $\mathbf{Z}$ (line 6). With this rearrangement, there will be a row in $\mathbf{Z}$ that carries the peaks of the sinc pulses, if present. However, in presence of a strong background noise (the case of interest in this work), these peaks may not be easily observable. Next, we add $\tau_w^{\max}$ to the index vector $\boldsymbol{\tau}$ and remove the oldest element from $\boldsymbol{\tau}$ (line 7). Finally, we declare that a packet is detected if K out of M elements in $\boldsymbol{\tau}$ are equal (line 8). Otherwise, we update the symbol index (line 11) and move on to the next symbol.

The analysis of Algorithm 1 is beyond the scope of this paper. Here, we only quote some theoretical results from our work [17] for the performance comparison with the simulation and experimental results presented in this paper. According to the formulae presented in [17], the choice of parameters $M = 8$ and $K = 6$ is a good compromise. A relatively small value of M means detection will be fast. Only a small data collection is needed to confirm the presence of the packet. This choice also results in a false alarm rate of around 10^{-9} (a packet is falsely detected when there is no packet). Fig. 2 presents the theoretical results of probability of missed detection of a packet for different choices of the parameter L and as a function of SNR. As seen, our packet detection algorithm can operate reliably at an SNR of $-10\,\mathrm{dB}$ or lower, confirming our claim that we have designed a reliable UCC. Also, the simulation and experimental results that are presented for the case $L = 128$ confirm the accuracy of our theoretical results.

Note that our novel timing acquisition and packet detection method distinguishes itself from traditional thresholding approaches (including their adaptive versions) that have been
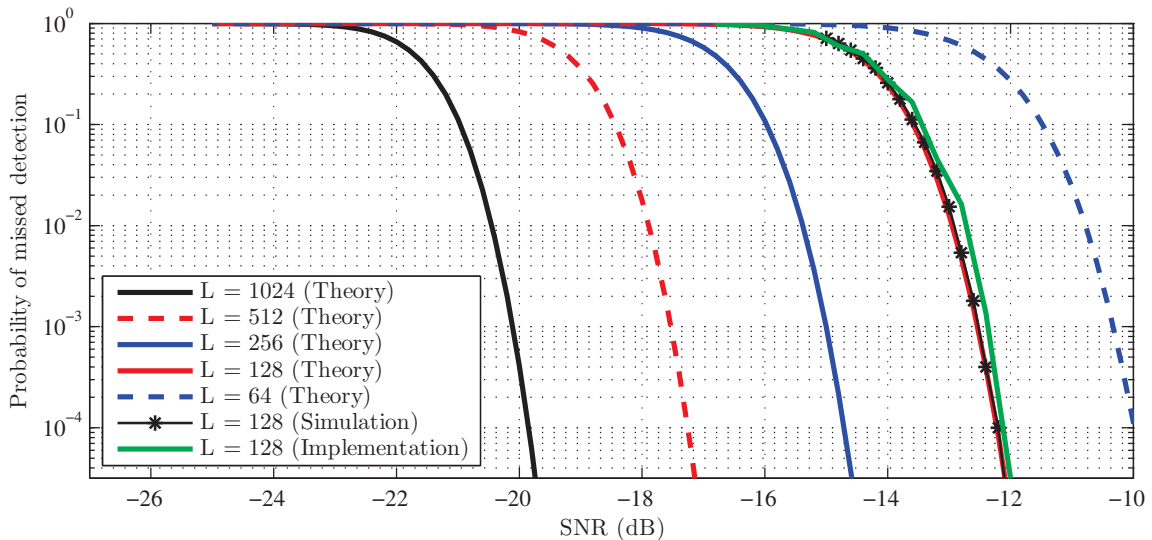
Fig. 2. Comparison of theoretical, simulation, and experimental results depicting probability of missed detection versus SNR(dB). Theoretical results are for various L while simulation and experimental results are for $L = 128$, $M = 8$, and $K = 6$

widely adopted for various spread spectrum systems in the past; e.g., see [18]–[24]. In our study, we found the thresholding methods are insufficient for typical scenarios of the UCC, which operates in a negative SNR environment and in the presence of high-power macro-cell transmissions. Moreover, due to the difficulty of the acquisition analysis, we limit our study to an additive white Gaussian noise (AWGN) environment. We acknowledge that in a real D2D communication scenario, where macro-cell users are present, this assumption does not remain valid. Nevertheless, we believe the insight provided by our study is sufficient to provide guidelines for application of the studied UCC in practical cognitive mesh networks.

VI. IMPLEMENTATION

Following the waveform structure and the packet format that were presented in the previous sections, an FB-MC-SS system was implemented on a National Instruments (NI) platform. The platform used consists of an NI FlexRIO FPGA Module (NI PXIe-7975R), which contains a Kintex-7 FPGA and 2 GB of onboard memory. This module is connected to an NI FlexRIO RF Transceiver (NI 5791R), which has a 130 MS/s 16 bit DAC for the transmitter (TX) and a 130MS/s 14 bit ADC for the receiver (RX). The RF Transceiver allows continuous frequency coverage from 200 MHz to 4.4 GHz, with 100 MHz of instantaneous bandwidth. The FPGA and Transceiver module are both connected to an NI real-time (RT) controller (NI PXIe-8135), which is used as a host PC and is programmed using NI LabVIEW Real-Time. We use two independent transceivers using the same setup described above to prototype the FB-MC-SS with two-way half-duplex communications.

A. Transmitter Implementation

The TX implementation is based on a polyphase structure whose detail can be found in [16]. Our implementation is based on an FFT size of $L = 128$, which occupies a total bandwidth of 32.5 MHz, if all subcarriers were in use. To allow guard bands at the two sides of the spectrum (for filtering operations), only the central 25 MHz of this bandwidth is used. Also, noting that, by design, FB-MC-SS only makes use of odd subcarriers, we end up with a design with a maximum number of active subcarrier of $N = 50$. We also note that, with $L = 128$ and a sampling rate of 32.5 MHz at the synthesis filter bank output, $T = 128/32.5 = 3.9385 \ \mu$s. Hence, the symbol rate in our design is $1/3.9385 \ \mu$s ≈ 254 ksymbols/s.

The TX generates the FB-MC-SS signal on the FPGA from the payload information it receives from the RT host. Spreading gain coefficients, γ_k's, are re-configurable from the RT host, and can be forced to zero to avoid interference with the active primary users. The output samples from the synthesis filter bank are up-sampled by a factor of 4 and interpolated to meet the DAC sampling rate requirement of 130 MS/s. VHDL (VHSIC Hardware Description Language) code is used to program the TX and RX designs onto the FlexRIO FPGA. Fig. 3 depicts pie charts, which show FPGA device utilization results for the following components on the FPGA: Slice Registers, Slice LUTs, Block RAMs, and DSP48s. The pie charts indicate how much of a given FPGA component is being used by our designs. We note that the compilation results of the TX and RX were obtained independently from one another.

B. Receiver Implementation

As is typical of most wireless communications designs, the receiver is the more complicated module to implement. The compilation results for the RX FPGA code are shown in Table I. A block diagram of the processing on the RX is shown in Fig. 4. The following steps are taken to recover
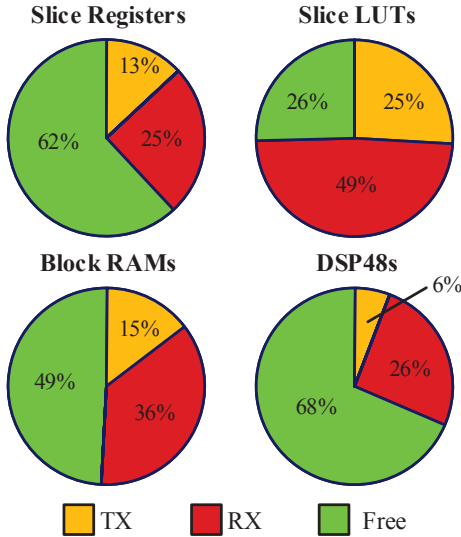
Fig. 3. Pie charts depicting the percentage of FPGA usage for TX and RX along with free area leftover on the FPGA.

TABLE I
RECEIVER DEVICE UTILIZATION

Device Utilization	Used	Total	Percent
Slice Registers	120097	508400	23.6
Slice LUTs	123689	254200	48.7
Block RAMs	288	795	36.2
DSP48s	394	1540	25.6

the information bits sent by the transmitter from the received signal after the ADC:

1) *Decimation:* A low-pass filter is used to reject the spectra out of the receiving signal band. The result is then decimated by a factor of 4. The output of this block, $y_{\text{dec}}[n]$, is a complex baseband signal with carrier frequency offset Δf_c.

2) *Demodulator:* The demodulator takes the averaged carrier frequency offset estimate, $E[\Delta \widetilde{f}_c]$, from the RT host, and corrects Δf_c present in the received signal using a Direct Digital Synthesizer (DDS). The output of this block is $y[n]$. Note that there still exists a residual carrier frequency offset $\Delta f_c^R = \Delta f_c - E[\Delta \widetilde{f}_c]$ due to the imperfection of the estimate.

3) *Matched Filter:* Passing $y[n]$ through a matched filter $g^*[-n]$, we get $y'[n]$, which, within the duration of the packet preamble, contains narrow sinc pulses at a spacing of L samples, as seen in (6) and (7).

4) *Packet Detection/Timing Recovery:* $y'[n]$ is passed to the packet detection and timing recovery block, whose detail of implementation was presented earlier in Section V. After a packet is detected, a command signal is passed to the subsequent blocks to start processing.

5) *Analysis Filter Bank:* Samples of $y[n]$, at the detected timing phase, are sent through a polyphase analysis filter bank, which consists of a polyphase filter and an L-point FFT block. This is similar to the analysis filter bank used in [16]. This block will output samples

$$\hat{s}_k[n] = C_k \gamma_k s[n] e^{j2\pi \Delta f_c^R n} + v_k \qquad (8)$$

where C_k is the channel response at subcarrier index k, v_k arises from the channel additive noise, and Δf_c^R is the residual carrier frequency offset.

6) *Despreader:* This block removes the spreading gain term γ_k from the right-hand side of (8), for all active subcarriers.

7) *Frequency Offset Estimation:* This module uses the preamble symbols to estimate Δf_c^R, denoted $\Delta \widetilde{f}_c$, and sends the estimate to the RT host. The RT host takes an average of $\Delta \widetilde{f}_c$ over many packets, and sends the average, $E[\Delta \widetilde{f}_c]$, to the demodulator. This module runs simultaneously with the Channel and Noise Estimation module.

8) *Channel and Noise Estimation:* This module estimates C_k and the noise variance, σ_k^2, at each subband using the known symbols in the preamble.

9) *MRC Gain Calculator:* The maximum ratio combiner (MRC) combines the analysis filter bank outputs to average out the noise and obtain a more reliable estimate of $s[n]$. See [16] for relevant equations.

10) *Adaptive MRC:* This module adapts the MRC coefficients over the length of the payload following a decision directed approach and using the normalized least mean square (NLMS) algorithm, [25].

11) *Payload Identifier:* The *payload indicator* word between the preamble and payload is detected at this module. Once the *indicator* word is detected, the remaining data is presumed to be payload data. This module is also used to correct any sign ambiguity that arises due to blind channel estimation in which the exact position of ±1 symbols in the preamble is unknown.

The RX continues to process each packet in the way described above independent of the previous packets. The only parameter that is tracked across packets is the frequency offset estimate $\Delta \widetilde{f}_c$. As a side-note, the descriptions of the blocks for flow control in the receiver implementation are beyond the scope of this paper.

VII. EXPERIMENTAL RESULTS

Tests are conducted to verify both the probability of missed detection and the probability of false alarm. In our RX implementation, the variables M and K were chosen to be 8 and 6, respectively. The SNR level is determined by the Channel and Noise Estimator module, and verified using a spectrum analyzer for one SNR level. After verification of this SNR level, we simply adjust the transmitter power to obtain different SNRs for our experimental results.

For each given SNR level, approximately 1 million packets are transmitted. A count of packets sent by the TX and detected packets at the RX is kept. The missed detection probability is calculated as the ratio of the number of packets
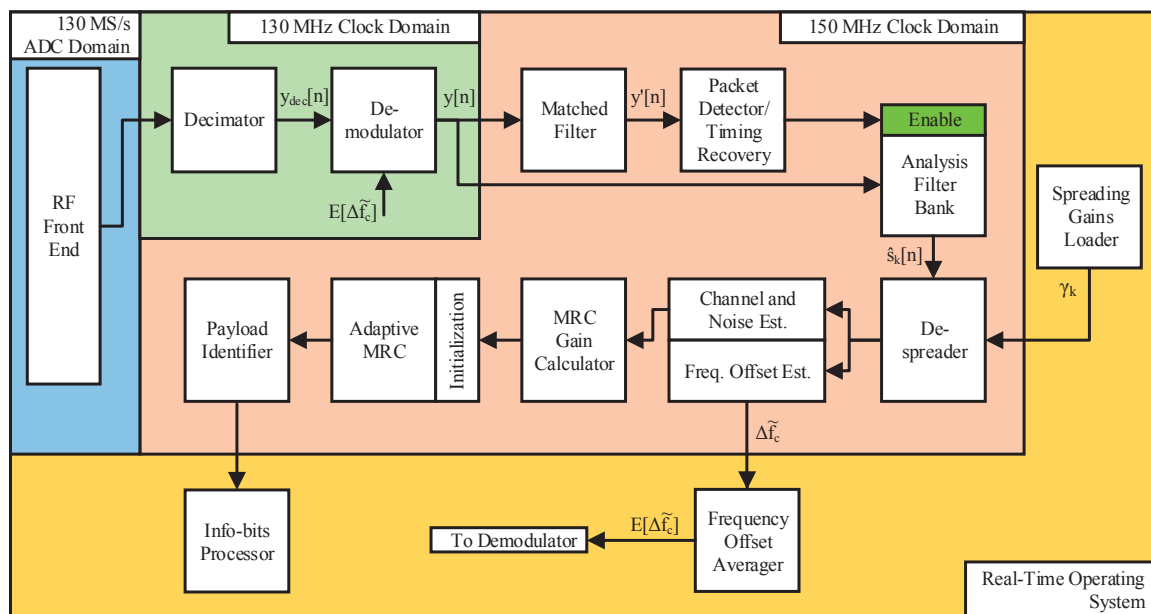
Fig. 4. Block diagram of the receiver implementation.

missed to the number of packets transmitted. The experiment is conducted over the range $[-16.8\,\text{dB}, -12.8\,\text{dB}]$ in increments of $0.4\,\text{dB}$.

A comparison of our experiment, simulation, and theoretical results can be seen in Fig. 2. This figure indicates that the theoretical and simulated results match well with one another, as do the experimental results within a fraction of a dB. This small difference can be attributed mainly to a sub-sample timing offset between the TX and RX. Although the clocks of both systems are synchronized, a difference in start-up times of the two systems causes an offset. The sub-sample timing offset causes the peaks of the pulses of the matched filter response to be lower in magnitude than the ideal scenario of no sub-sample offset. Aside from this, other implementation specific details such as quantization noise, differences in RF hardware, etc. can also contribute to differences we see in Fig. 2.

VIII. Cognitive Mesh Networks

In previous sections, we presented the packet format and the packet detection method for our proposed UCC. In this section, we discuss how our proposed preamble design and packet detection facilitate control message exchanges and achieve reliable communications in 5G cognitive mesh networks.

The constant availability of control channels in 5G D2D communications provides the common medium for D2D UEs to cooperate and exchange control messages efficiently without having to consume macro-cell control resources or spend time on finding where in the spectrum to transmit the control information. This is especially valuable for D2D communications between UEs from multi-tier cells or even from different network operators. Specifically, for the UCC to remain constantly available, all D2D UE transmissions on the UCC needs to be robust to both cellular-to-D2D interference and D2D-to-D2D

interference. The robustness to interference of the proposed UCC is obtained by the processing gain of the FB-MC-SS waveforms. The larger the number of subcarriers, the higher the processing gain given the same subcarrier spacing. For example, by increasing the number of subcarriers from 50 to 500, we obtain an extra $10\,\text{dB}$ of processing gain. Therefore, it is achievable to have reliable transmissions below the noise floor ($-10\,\text{dB} \sim -20\,\text{dB}$), which makes the UCC virtually always available for exchanging control messages and data among cognitive mesh network users.

For neighbor discovery in cognitive mesh networks, the proposed UCC simplifies the active or passive scanning procedures with faster probe response time because all mesh users can transmit beacons or send probe requests and responses using the same control channel. To avoid the collisions of beacons and control packets, the mesh users can synchronize among themselves by using a synchronization mechanism similar to IEEE 802.11 neighbor offset synchronization, and adopt a collision avoidance method such as IEEE 802.11 mesh beacon collision avoidance (MBCA) [26]. These operations rely on beacon exchanges with important timing information for synchronizing neighboring mesh users. As a result, the proposed underlay control channel is indispensable for the reliable and efficient delivery of these beacons among mesh users. The self-forming and self-organizing capabilities of cognitive mesh users significantly offload the control overhead of macro-cells or small cells in 5G wireless systems.

Once the neighboring mesh users are synchronized, they are able to reserve and schedule the channel access opportunities by using the contention free channel access scheme. Alternatively, mesh users can gain access to the channel by using the contention-based channel access such as carrier sense

multiple access with collision avoidance (CSMA/CA) [26]. As a result, the hidden node problem in mesh networks can be mitigated by these collision avoidance schemes: MBCA for control transmissions and CSMA/CA for data transmissions, both of which can be realized by utilizing the same proposed UCC physical layer packet format and packet detection method for D2D communications.

Lastly, the proposed UCC is crucial for efficient routing operations such as route setup and updates in mesh networks. Mesh networks are multi-hop networks in which mesh users relay packets from the source to the destination by either using the established routes (proactive routing) or determining the path hop-by-hop (reactive routing). The proactive routing requires the route setup and constant route updates for maintaining the best routing paths, whereas the reactive routing algorithms search routes by sending route requests to all users in the mesh networks. Hence, either type of routing algorithms can utilize the UCC to leverage the efficiency of routing. Needless to say, the routing efficiency of the hybrid routing approaches similar to the Hybrid Wireless Mesh Protocol [26] can also be enhanced by the constantly available UCC.

IX. Conclusion

In this paper, we proposed an underlay communication channel (UCC) based on filter bank multicarrier spread spectrum for 5G cognitive mesh networks. We also proposed a new packet format and a novel timing acquisition and packet detection method to facilitate reliable D2D UE communications in such networks. The design implemented was tailored towards operating while hidden under the channel noise. This makes it an ideal candidate for UCC operations in a mesh network, as it introduces minimum spectral taxation to macro-cell/small-cell base stations and their UEs. The validity of our work was confirmed through simulations and experimental results. Finally, we developed a complete receiver design on a software radio platform and showed our receiver design occupies approximately 50% of a Xilinx Kintex-7 FPGA chip.

Acknowledgment

References

[1] M. Sherman, A. N. Mody, R. Martinez, C. Rodriguez, and R. Reddy, "IEEE standards supporting cognitive radio and networks, dynamic spectrum access, and coexistence," *IEEE Communications Magazine*, vol. 46, no. 7, pp. 72–79, Jul. 2008.

[2] C. R. Stevenson, G. Chouinard, Z. Lei, W. Hu, S. J. Shellhammer, and W. Caldwell, "IEEE 802.22: The first cognitive radio wireless regional area network standard," *IEEE Communications Magazine*, vol. 47, no. 1, pp. 130–138, Jan. 2009.

[3] M. Song, C. Xin, Y. Zhao, and X. Cheng, "Dynamic spectrum access: from cognitive radio to network radio," *IEEE Wireless Communications*, vol. 19, no. 1, pp. 23–29, Feb. 2012.

[4] T. Yucek and H. Arslan, "A survey of spectrum sensing algorithms for cognitive radio applications," *IEEE Communications Surveys & Tutorials*, vol. 11, no. 1, pp. 116–130, First 2009.

[5] S. Haykin, "Cognitive radio: brain-empowered wireless communications," *IEEE Journal on Selected Areas in Communications*, vol. 23, no. 2, pp. 201–220, Feb. 2005.

[6] E. Axell, G. Leus, E. G. Larsson, and H. V. Poor, "Spectrum sensing for cognitive radio: State-of-the-art and recent advances," *IEEE Signal Processing Magazine*, vol. 29, no. 3, pp. 101–116, May 2012.

[7] Y. C. Liang, K. C. Chen, G. Y. Li, and P. Mahonen, "Cognitive radio networking and communications: an overview," *IEEE Trans. on Vehicular Technology*, vol. 60, no. 7, pp. 3386–3407, Sept. 2011.

[8] B. Farhang-Boroujeny, "Filter bank spectrum sensing for cognitive radios," *IEEE Transactions on Signal Processing*, vol. 56, no. 5, pp. 1801–1811, May 2008.

[9] B. F. Lo, "A survey of common control channel design in cognitive radio networks," *Physical Communication*, vol. 4, no. 1, pp. 26–39, Mar. 2011.

[10] J. Liu, N. Kato, J. Ma, and N. Kadowaki, "Device-to-device communication in LTE-Advanced networks: A survey," *IEEE Communications Surveys & Tutorials*, vol. 17, no. 4, pp. 1923–1940, Fourthquarter 2015.

[11] S. Hara and R. Prasad, "Overview of multicarrier CDMA," *IEEE Communications Magazine*, vol. 35, no. 12, pp. 126–133, Dec. 1997.

[12] S. Kondo and B. Milstein, "Performance of multicarrier DS CDMA systems," *IEEE Trans. on Communications*, vol. 44, no. 2, pp. 238–246, Feb. 1996.

[13] G. K. Kaleh, "Frequency-diversity spread-spectrum communication system to counter bandlimited Gaussian interference," *IEEE Trans. on Communications*, vol. 44, no. 7, pp. 886–893, Jul. 1996.

[14] K. Cheun, K. Choi, H. Lim, and K. Lee, "Antijamming performance of a multicarrier direct-sequence spread-spectrum system," *IEEE Trans. on Communications*, vol. 47, no. 12, pp. 1781–1784, Dec. 1999.

[15] B. Farhang-Boroujeny and C. Furse, "A robust detector for multicarrier spread spectrum transmission over partially jammed channels," *IEEE Trans. on Signal Processing*, vol. 53, no. 3, pp. 1038–1044, Mar. 2005.

[16] D. Wasden, H. Moradi, and B. Farhang-Boroujeny, "Design and implementation of an underlay control channel for cognitive radios," *IEEE Journal on Selected Areas in Communications*, vol. 30, no. 10, pp. 1875–1889, Nov. 2012.

[17] T. Sibbett, H. Moradi, and B. Farhang-Boroujeny, "Design and analysis of a novel timing acquisition method for spread-spectrum systems," submitted for publication, 2016.

[18] D. L. Noneaker, A. R. Raghavan, and C. W. Baum, "The effect of automatic gain control on serial, matched-filter acquisition in direct-sequence packet radio communications," *IEEE Trans. on Vehicular Technology*, vol. 50, no. 4, pp. 1140–1150, Jul. 2001.

[19] U. Madhow and M. B. Pursley, "Acquisition in direct-sequence spread-spectrum communication networks: an asymptotic analysis," *IEEE Trans. on Information Theory*, vol. 39, no. 3, pp. 903–912, May 1993.

[20] P. F. Driessen and Z. L. Shi, "A new rapid acquisition scheme for burst mode DS spread spectrum packet radio," in *Proc. IEEE Military Communications Conference*, Nov. 1991, pp. 809–813 vol.2.

[21] J. Y. Kim and J. H. Lee, "Parallel acquisition scheme for direct-sequence spread-spectrum multiple-access packet radio communication," *Electronics Letters*, vol. 31, no. 12, pp. 948–950, Jun. 1995.

[22] R. D. Gaudenzi, F. Giannetti, and M. Luise, "Signal recognition and signature code acquisition in CDMA mobile packet communications," *IEEE Trans. on Vehicular Technology*, vol. 47, no. 1, pp. 196–208, Feb. 1998.

[23] M. Amde, J. Marciano, R. Cruz, and K. Yun, "Code acquisition at low SINR in spread spectrum communications," in *Proc. IEEE Ninth Int'l Symposium on Spread Spectrum Techniques and Applications*, Aug. 2006, pp. 470–475.

[24] A. Swaminathan and D. L. Noneaker, "A technique to improve the performance of serial, matched-filter acquisition in direct-sequence spread-spectrum packet radio communications," *IEEE Journal on Selected Areas in Communications*, vol. 23, no. 5, pp. 909–919, May 2005.

[25] B. Farhang-Boroujeny, *Adaptive Filters: Theory and Applications*, 2nd ed. John Wiley & Sons, 2013.

[26] "IEEE Standard for Information Technology–Telecommunications and Information Exchange between Systems Local and Metropolitan Area Networks–Specific Requirements Part 11: Wireless LAN Medium Access Control (MAC) and Physical Layer (PHY) Specifications," *IEEE Std 802.11-2012*, pp. 1–2793, Mar. 2012.